Observation of Discrete Solitons and Soliton Rotation in Optically Induced Periodic Ring Lattices

Article *in* Physical Review Letters · April 2006

DOI: 10.1103/PhysRevLett.96.083904 · Source: PubMed

3 authors, including:

Xiaosheng Wang
Xiangya Hospital of Central South University
32 PUBLICATIONS **872** CITATIONS

SEE PROFILE

Zhigang Chen
San Francisco State University
496 PUBLICATIONS **10,865** CITATIONS

SEE PROFILE

Observation of Discrete Solitons and Soliton Rotation in Optically Induced Periodic Ring Lattices

Xiaosheng Wang[1,2] and Zhigang Chen[1,3]

[1]*Department of Physics and Astronomy, San Francisco State University, San Francisco, California 94132, USA*
[2]*The State Key Lab of Optoelectronic Materials and Technologies, Sun Yat-sen University, Guangzhou, China*
[3]*TEDA Applied Physical School, Nankai University, Tianjin, China*

P. G. Kevrekidis

Department of Mathematics and Statistics, University of Massachusetts, Amherst, Massachusetts 01003, USA
(Received 26 October 2005; published 3 March 2006)

We report the first experimental demonstration of ring-shaped photonic lattices by optical induction and the formation of discrete solitons in such radially symmetric lattices. The transition from discrete diffraction to single-channel guidance or nonlinear self-trapping of a probe beam is achieved by fine-tuning the lattice potential or the focusing nonlinearity. In addition to solitons trapped in the lattice center and in different lattice rings, we demonstrate controlled soliton rotation in the Bessel-like ring lattices.

DOI: 10.1103/PhysRevLett.96.083904 PACS numbers: 42.65.Tg, 05.45.Yv

Nonlinear periodic structures or discrete systems are abundant in nature. A typical example in optics is the waveguide lattice either manually fabricated or optically induced in nonlinear media. Such waveguide lattices provide a benchmark for studying many intriguing phenomena of light propagation mediated by discreteness and nonlinearity. Among them are the intrinsic localized modes or the so-called discrete solitons (DS), which have attracted great attention not only in optics [1,2] but also in other diverse fields such as biology [3], solid state physics [4], micromechanical systems [5], and Bose-Einstein condensates [6]. Even in optics, DS have been demonstrated experimentally in a variety of settings, including semiconductor waveguide arrays with Kerr nonlinearity [7], optically induced waveguide lattices with photorefractive nonlinearity [8–10], fabricated channel waveguides in lithium niobate crystals with quadratic nonlinearity [11], and voltage-controlled waveguide arrays in liquid crystals with orientational nonlinearity [12]. Thus far, all experimental work on DS has been performed either on one-dimensional (1D) lattices or on two-dimensional (2D) lattices with no rotational symmetry (e.g., square lattices).

On the other hand, in the 2D domain, many fundamental features are expected to occur not only because lattice structures can be richly configured with different lattice symmetry, but even in a given lattice symmetry (such as in square lattices) spatial solitons that have no analog in the 1D domain can be realized. Typical examples are the discrete solitons that carry angular momentum [13,14] or that have a nontrivial intensity or phase structures [15]. When rotational symmetry is desired, one can have another important class of lattices such as those created by nondiffracting Bessel beams [16]. As recently proposed by Kartashov *et al.*, such lattice symmetry may lead to new soliton features attractive for applications in soliton manipulation including the possibility to induce rotary soliton motions and reconfigurable soliton networks [17].

In this Letter, we demonstrate for the first time the formation of Bessel-like photonic lattices by optical induction. Such ring-shaped lattices remain nearly invariant in a 10 mm long photorefractive nonlinear crystal. Discrete diffraction and discrete solitons are observed when a probe beam is launched both into the lattice center and into different lattice rings. In the former case (center excitation), we demonstrate a clear transition from discrete diffraction to linear single-channel guidance by fine-tuning the lattice potential and to nonlinear self-trapping of the probe beam by fine-tuning the self-focusing nonlinearity. In the latter case (off-center excitation), we also demonstrate controlled soliton rotation in different lattice rings by imposing an initial transverse momentum to the soliton. Our experimental results are in good agreement with the theoretical analysis of these effects. These rotary solitons are expected to play new roles in soliton-driven photonics, and their experimental realization might provide insight into similar phenomena in other nonlinear systems of periodic ring structures.

Our experimental setup is illustrated in Fig. 1(a). Different from what was used earlier for the generation of soliton pixels [18] and DS in square lattices [10,14,15], here we use an amplitude mask with an equally spaced concentric ring pattern. A coherent laser beam operating at 532 nm wavelength is split into two beams by a polarizing beam splitter (PBS) before entering into a 10 mm long SBN (strontium barium niobate) photorefractive crystal. The lattice-forming beam passing through the mask is ordinarily polarized (*o* beam), and the soliton-forming beam is extraordinarily polarized (*e* beam). When the mask is imaged onto the input face of the crystal, a spatial bandpass filter is introduced in the Fourier plane. After proper filtering, the mask gives rise to a Bessel-like intensity pattern at the crystal input [Fig. 1(b)], which remains nearly invariant during linear propagation. We note that the ring pattern created this way is slightly different from the true Bessel pattern, since both the intensity and the spacing between

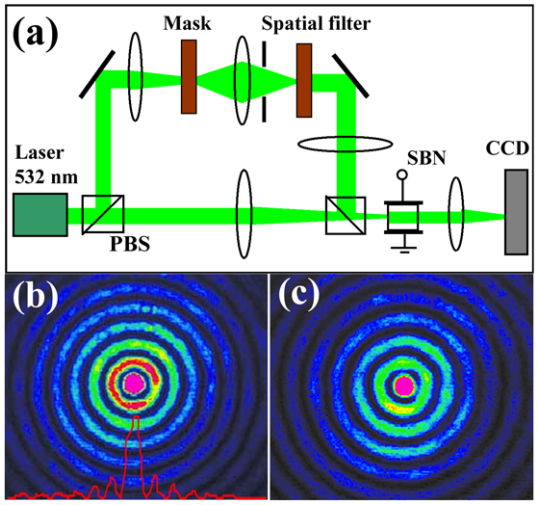

FIG. 1 (color online). (a) Experimental setup. (b),(c) Intensity patterns of ring lattice at crystal (b) input and (c) output with a 4.0 kV/cm bias field. Superimposed in (b) is the transverse intensity profile of the ring lattice.

adjacent rings do not decrease so dramatically in the radial direction. (In fact, the true Bessel pattern has a normalized intensity of 1.00, 0.15, 0.09, and 0.06 for the first four maxima, while our measured normalized intensity is 1.00, 0.25, 0.14, and 0.10. Starting from the first ring, the measured spacing between adjacent rings is about 20 μm even far away from the center.) With an appropriate bias field, such a ring pattern from the o beam induces a periodic ring waveguide lattice that propagates nearly linearly throughout the 10 mm long crystal [as shown in Fig. 1(c)]. To fine-tune the lattice potential and the nonlinearity of the probe beam, a background illumination from an incandescent lamp is used to cover the entire crystal from the top.

In an anisotropic photorefractive crystal, the nonlinear index change experienced by an optical beam depends on its polarization as well as on its intensity. Under appreciable bias conditions, i.e., when the photorefractive screening nonlinearity is dominant, this index change is approximately given by $\Delta n_e = (n_e^3 r_{33} E_0/2)(1 + I)^{-1}$ and $\Delta n_o = [n_o^3 r_{13} E_0/2](1 + I)^{-1}$ for e-polarized and o-polarized beams, respectively [8–10]. Here E_0 is the applied electric field along the crystalline c axis, (n_e, r_{33}) and (n_o, r_{13}) are the unperturbed indices and electro-optic coefficients corresponding to e beam and o beam, respectively, and I is the intensity of the beam normalized to the background illumination. In our SBN crystal, r_{13} is about 10 times smaller than r_{33}, yet the o-polarized Bessel-like beam induces an appreciable index change Δn_o necessary for forming the ring waveguide lattice. As established earlier [19], the width and the depth of induced waveguides depend critically on the normalized intensity when other parameters such as the bias field are fixed. By changing the background illumination, which changes the normalized intensity when the lattice intensity is fixed, we can effectively fine-tune the waveguide potential so as to adjust the lattice coupling. Since the intensity at the center of the lattice is much stronger than that in different rings [Figs. 1(b) and 1(c)], the probe beam (aimed into the center) tends to be guided in the center if the coupling between surrounding ring waveguides is not strong. On the other hand, if the waveguide coupling is strong, discrete diffraction to the rings and guidance to the central lattice core will compete. Based on this, we observed a transition from discrete diffraction to single-channel guidance of the probe beam simply by changing the level of background illumination. Typical results are illustrated in Fig. 2, where Figs. 2(a)–2(c) show the output intensity patterns of the probe beam as the intensity of background illumination is set at a different level. The peak intensity ratio between the central core of the lattice beam and the probe beam is about 7:1, and the applied dc field is 3.80 kV/cm. When the background illumination is very weak [Fig. 2(a)], the coupling between the central waveguide and the ring channel waveguides is strong, so the probe beam undergoes discrete diffraction. We can see that the energy of the probe beam tunnels to several surrounding rings. As the background intensity is increased, the depth and width of the lattice waveguide decrease, so the coupling gets weaker and the probe beam is more guided to the central waveguide [Fig. 2(b)]. When the background illumination is very high, the waveguide coupling in lattice rings becomes very weak, so the guidance of the probe beam into the central core dominates [Fig. 2(c)]. For comparison, the

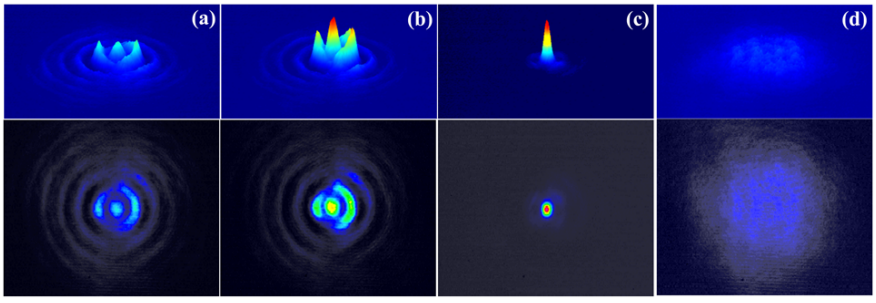

FIG. 2 (color online). Transition from discrete diffraction (a) to central channel guidance (c) of a probe beam in ring lattice. From (a) to (c), the background illumination is enhanced gradually while all other conditions unchanged, and (d) shows that the probe beam has no nonlinear self-action under the same bias condition without lattice. Top: 3D intensity plots; bottom: corresponding 2D transverse patterns. For better visualization, the contrast of images is slightly adjusted [the peak intensity ratio between (a) and (c) is 1:12].

normal diffraction of the probe beam without lattice under the same bias condition is illustrated in Fig. 2(d), showing no nonlinear self-action of the probe beam itself at this experimental condition. Thus, the transition between multichannel diffraction and single-channel guidance occurs while the probe beam undergoes linear propagation and is achieved here merely by varying the background illumination. Although the rings in an *o*-polarized lattice beam appear to retain good circular symmetry (Fig. 1), the rings in an *e*-polarized probe beam break slightly (Fig. 2) due to the anisotropic photorefractive nonlinearity.

Next we show nonlinear propagation of the probe beam that leads to formation of DS in the ring lattice. To do so, we raised the intensity of the probe beam to be much higher than that of the lattice. When the probe beam experiences nonlinear self-action, the self-focusing of the probe beam and the waveguide coupling will compete. Under proper conditions, a balance between self-focusing and discrete diffraction can be reached which results in formation of DS. To ensure trapping of the probe beam results from nonlinear self-action rather than simple guidance, we take advantage of the noninstantaneous nature of the photorefractive nonlinearity. Experimental results are illustrated in Fig. 3, where (a) and (c) show the linear diffraction patterns which were taken 0.05 s after the probe beam (11.5 μm, FWHM) was launched into the lattice (before self-action took place), and (b) and (d) show the corresponding self-trapped patterns taken 60 s later when the crystal has reached a new steady state. For on-center excitation [Fig. 3, top], the peak intensity ratio between the central core of the lattice and the probe beam is about 1:4, and the applied dc field is 3.00 kV/cm. For off-center excitation [Fig. 3, bottom] where the probe is aimed at the third ring, the intensity ratio between the third lattice ring and the probe beam is about 1:8, and the applied field is 3.80 kV/cm. As seen from these figures, the probe beam undergoes strong discrete diffraction before nonlinear self-action takes place, with the diffracted beam covering several lattice rings, but its energy becomes much more localized due to nonlinear self-trapping. We emphasize that the results in Fig. 3 are fundamentally different from those in Fig. 2, as the latter were obtained merely due to linear waveguiding in the lattice center.

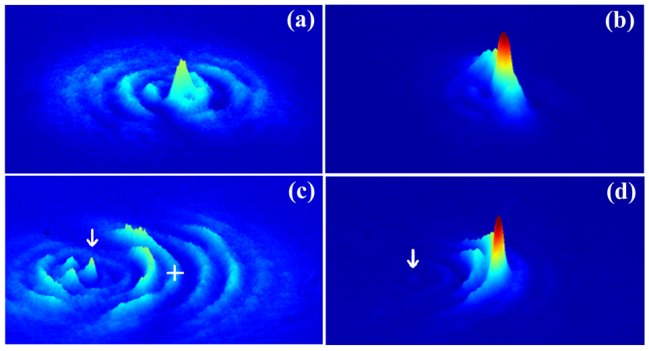

FIG. 3 (color online). Transition from discrete diffraction (a),(c) to nonlinear self-trapping (b),(d) of a probe beam launched in the center (a),(b) and the third ring (c),(d) of the lattice. Patterns in (a),(c) were taken instantaneously (<0.1 s) while those in (b),(d) were taken in steady state. The arrow indicates the center of the ring lattice, and the cross indicates the input position of the probe beam.

The above experimental observations are corroborated by numerical simulations. A theoretical model based on beam propagation with a photorefractive screening nonlinearity and a periodic lattice potential can account for the basic features observed in our experiments. The nondimensional equation for the propagation is of the form [20]

$$iU_z + U_{xx} + U_{yy} - \frac{E_0}{1 + I_l + |U|^2} U = 0, \qquad (1)$$

where U is the normalized amplitude of the probe beam, and I_l is the ring lattice intensity from a true Bessel beam. Similar to that used in experiment, the distance between the central core and the first ring is set to be 20 μm. z is the normalized propagation distance, and E_0 is the applied dc field in the units of $1/(k_0^2 n_e^4 r_{33})$. Typical results using parameters close to those from experiment are shown in Fig. 4 for cases when the Gaussian probe beam is launched near the lattice center (top panels) as well as far away from the center (bottom panels). The left panels show the evolution of the probe beam in the absence of nonlinearity, while the right panels illustrate the self-focusing effect in the presence of the nonlinearity that leads to discrete solitons localized on the corresponding lattice ring. As noted before, in a Bessel function the amplitude drops much faster in the radial direction than that in the Bessel-like pattern created in our experiment. As such, confine-

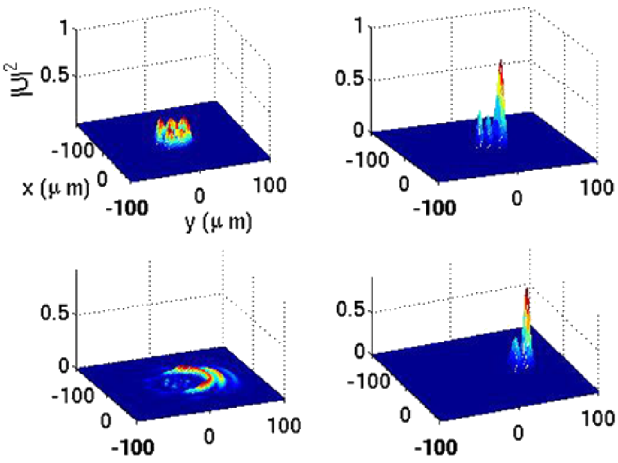

FIG. 4 (color online). Numerical results obtained using parameters close to those in Fig. 3. Patterns were taken after 10 mm of propagation corresponding to crystal length when the nonlinearity is (left) absent and (right) present. The probe was launched (top) 20 and (bottom) 48 μm away from the center, corresponding to excitations near the center and near the third ring. A true Bessel lattice has been used in numerical simulations.

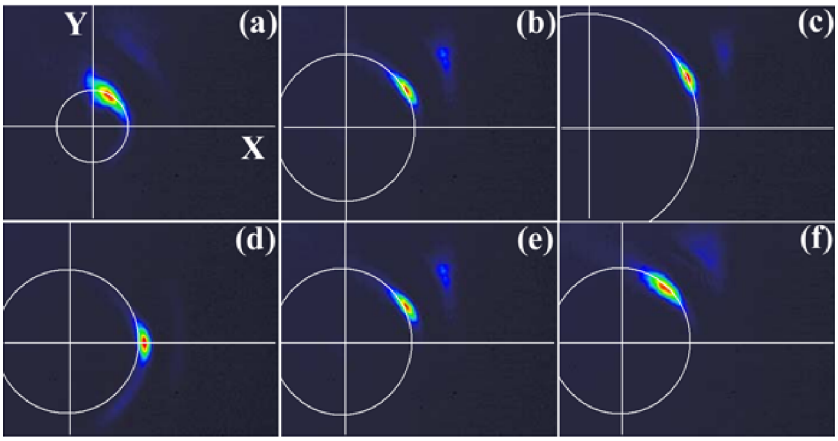

FIG. 5 (color online). Soliton rotation in the ring lattice. From (a) to (c), the probe was aimed at the far right side of the first, second, and third ring with the same tilting angle (about 0.4°) in the y direction. From (d) to (f), the probe was aimed at the same second ring but with different tilting angles of 0°, 0.4°, and 0.6°, respectively.

ment of the probe beam excited near the lattice center is found in our simulation even when the nonlinearity is turned off. In fact, if the probe beam is excited exactly in the lattice center, it experiences strong linear guidance into the center site in a truly Bessel lattice. Such behavior of the probe beam in the Bessel lattices has been found with Kerr nonlinearity by Kartashov *et al.* [16], while here we illustrate that such solutions persist in the presence of a photorefractive screening nonlinearity by using parameters close to those from the experiment.

A fascinating property of solitons particular to the setting of ring lattices is that such solitons can rotate around the rings without much radiation during their rotary motion [16]. To demonstrate such soliton rotation experimentally, we launch the probe beam on the far right side of the ring with a tilting angle towards the y direction, thus imposing an initial transverse momentum to the probe. We observe that the degree of soliton rotation increases with the tilting angle for the same ring excitation but decreases as the soliton is created at the larger rings. Figure 5 shows the rotary motion of the soliton in different rings with the same tilting angle (top panel) and in the same ring with different tilting angles (bottom panel). For these experimental results, the space between the rings is about 40 μm, the intensity ratio between the ring which the soliton locates and the peak of the probe beam is about 4:9, and the applied dc field is 5.2 kV/cm. From Fig. 5, we see clearly that the probe beam with a tilting angle can form a spatial soliton that rotates along the ring in which it is created. Furthermore, with the same tilting angle, the rotary angle decreases as the soliton is excited in the outer rings, as expected from particle rotation. Similar results have also been obtained in our numerical simulations.

In conclusion, we have demonstrated the formation of optically induced ring photonic lattices with radial symmetry and observed rotary discrete solitons in such lattices. The controlled transition from discrete diffraction to the center-core guidance is realized, which may find application in optical limiting and all-optical switching. Radially symmetric (or asymmetric) discrete diffractions and discrete solitons are observed for on-center (or off-center) excitations. In addition, soliton rotation in different lattice rings with different initial conditions is demonstrated. Our experimental findings with photonic ring lattices may prove to be relevant to similar phenomena in other nonlinear systems such as Bose-Einstein condensates trapped in ring-shaped magnetic waveguides [21].

This work was supported by the National Science Foundation, the Air Force Office of Scientific Research, the Petroleum Research Fund, and the National Natural Science Foundation of China (60328406).

[1] D. N. Christodoulides and R. I. Joseph, Opt. Lett. **13**, 794 (1988); D. N. Christodoulides *et al.*, Nature (London) **424**, 817 (2003).
[2] Y. S. Kivshar and G. P. Agrawal, *Optical Solitons* (Academic, New York, 2003).
[3] A. Xie *et al.*, Phys. Rev. Lett. **84**, 5435 (2000); J. Edler *et al.*, *ibid.* **93**, 106405 (2004).
[4] A. J. Sievers and S. Takeno, Phys. Rev. Lett. **61**, 970 (1988); B. I. Swanson *et al.*, *ibid.* **82**, 3288 (1999).
[5] M. Sato *et al.*, Phys. Rev. Lett. **90**, 044102 (2003).
[6] A. Trombettoni and A. Smerzi, Phys. Rev. Lett. **86**, 2353 (2001).
[7] H. S. Eisenberg *et al.*, Phys. Rev. Lett. **81**, 3383 (1998); R. Morandotti *et al.*, *ibid.* **83**, 2726 (1999).
[8] J. W. Fleischer *et al.*, Nature (London) **422**, 147 (2003).
[9] D. Neshev *et al.*, Opt. Lett. **28**, 710 (2003).
[10] H. Martin *et al.*, Phys. Rev. Lett. **92**, 123902 (2004).
[11] R. Iwanow *et al.*, Phys. Rev. Lett. **93**, 113902 (2004).
[12] A. Fratalocchi *et al.*, Opt. Lett. **29**, 1530 (2004).
[13] B. A. Malomed and P. G. Kevrekidis, Phys. Rev. E **64**, 026601 (2001); J. Yang and Z. H. Musslimani, Opt. Lett. **28**, 2094 (2003).
[14] D. N. Neshev *et al.*, Phys. Rev. Lett. **92**, 123903 (2004); J. W. Fleischer *et al.*, *ibid.* **92**, 123904 (2004).
[15] Z. Chen *et al.*, Phys. Rev. Lett. **92**, 143902 (2004); J. Yang *et al.*, *ibid.* **94**, 113902 (2005).
[16] Y. V. Kartashov *et al.*, Phys. Rev. Lett. **93**, 093904 (2004).
[17] Y. V. Kartashov *et al.*, Opt. Lett. **30**, 637 (2005); Z. Xu *et al.*, *ibid.* **30**, 1180 (2005).
[18] Z. Chen and K. McCarthy, Opt. Lett. **27**, 2019 (2002).
[19] M. Shih *et al.*, J. Opt. Soc. Am. B **14**, 3091 (1997).
[20] J. Yang, New J. Phys. **6**, 47 (2004).
[21] S. Gupta *et al.*, Phys. Rev. Lett. **95**, 143201 (2005).